Bulletin of Engineering Geology and the Environment (2020) 79:355–370
https://doi.org/10.1007/s10064-019-01547-6

ORIGINAL PAPER

Experimental triaxial testing of swelling gouge materials

Are Håvard Høien [1,2] · Bjørn Nilsen [1] · Gunnar Vistnes [1] · Roger Olsson [3]

Received: 6 December 2018 / Accepted: 12 May 2019 / Published online: 27 May 2019

Abstract

Adequate rock support in weakness zones that may contain swelling minerals poses one of the main challenges of excavating tunnels in hard rock conditions. Deformations under such conditions are influenced by several factors, including the properties of the rock mass, rock stress and the possible swelling potential of the minerals. Thus, dimensioning rock support may be challenging. To increase the knowledge regarding the processes behind deformations in areas of swelling gouge material, an experimental triaxial laboratory test of such material was performed. The main objective was to investigate whether the material might exert pressure under typical in situ stress conditions, or whether other processes might be dominant. In addition, the possible elastic and strength properties of such material were investigated. The testing was performed on reconstituted cores with material from four different locations in eastern Norway. The material was dried and then pressed into cores using a compactor. The triaxial testing consisted of four successive phases: pre-stressing 1; water addition under constant strain; pre-stressing 2 and failure. The results indicate that factors other than swelling pressure are the main causes of tunnel deformation, as no build-up of swelling pressure was observed during the water addition phase. Initially, the E-modulus and strength properties of the samples were very low, which can cause large, immediate deformations in situ. In addition, creep and possibly a reduction in the E-modulus during water addition seemed to cause time-dependent deformation.

Keywords Swelling · Swelling gouge · Weakness zone · Triaxial test · Deformation

Introduction

A frequent major challenge during tunnelling in hard rock conditions is related to weakness zones containing swelling minerals. Time-dependent deformations, such as swelling and squeezing, are particularly difficult to cope with. The dimensioning of rock support under such conditions is a challenging task, since these deformations are influenced by various factors, including rock mass quality, rock stresses and swelling pressure. To increase the knowledge of the process behind these deformations regarding swelling, an experimental triaxial laboratory test of reconstituted cores of swelling gouge material has been performed.

A weakness zone gouge may have properties varying within wide ranges, and in many cases it has a character similar to a moraine. The gouge represents a mix of grain sizes ranging from clay to gravel, and even blocks, and with low to no degree of bonding between the individual grains (Rokoengen 1973). As will be shown later, materials tested in this study are categorized as sandy, gravely and clayey. For materials of this category, the pore pressure and the flow of water may be of great significance with respect to the deformations.

Basically, there are two main types of deformations: immediate and time-dependent (Terzaghi and Peck 1967; Bellwald 1990; Barla 1999); see Fig. 1. The immediate deformations are caused by the in situ stress, and stress changes that occur due to tunnel excavation, and are dependent on the elastic and plastic mechanical properties of the material. These deformations, which occur in the undrained phase, may result in positive and negative excess pore pressures around the tunnel when

Electronic supplementary material The online version of this article (https://doi.org/10.1007/s10064-019-01547-6) contains supplementary material, which is available to authorized users.

✉ Are Håvard Høien
are.hoien@vegvesen.no

[1] Norwegian University of Science and Technology, Sem Sælands veg 1, 7491 Trondheim, Norway

[2] Norwegian Public Roads Administration, Postboks 8142 Dep, 0033 Oslo, Norway

[3] Norwegian Geotechnical Institute, P.O. Box. 3930, Ullevål Stadion, 0806 Oslo, Norway

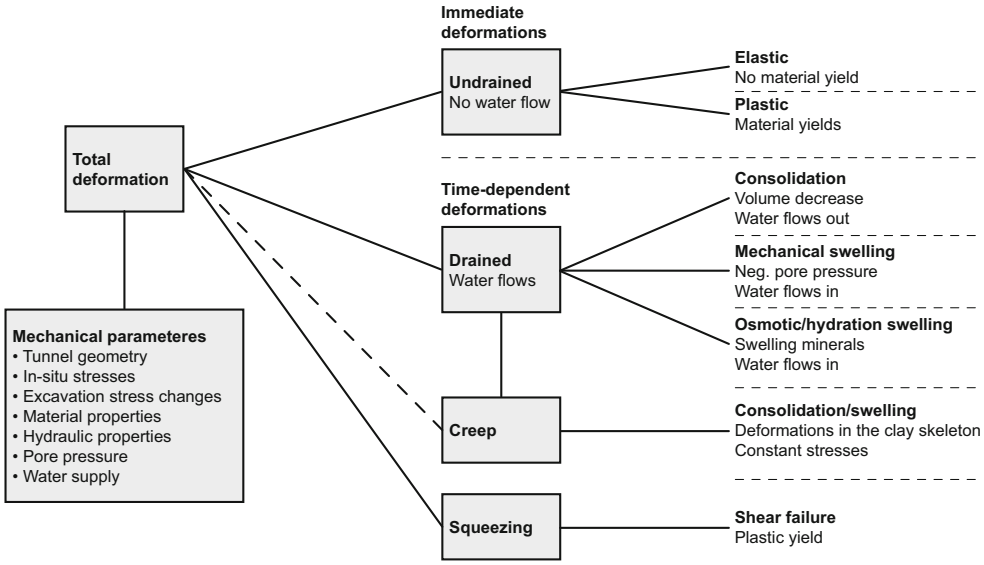

Fig. 1 Types of deformation in weakness zones. Due to the different stress states around a tunnel, different processes may take place at the same time at different locations, and even more than one may occur at the same location

the material has a large portion of fine grains. The main types of time-dependent deformations are (mineral) swelling, squeezing, creep, consolidation and mechanical swelling. If certain conditions are present, drained behaviour may occur, and as Bellwald (1990) pointed out, the material will either swell or consolidate depending on whether water flows into the material (negative excess pore pressure) or out of it (positive excess pore pressure), resulting in a volume increase or decrease.

The two main categories of mineral swelling for a gouge material are hydration and osmotic (Barla 1999; Einstein 1996; Bellwald 1990; Selmer-Olsen 1985; Aristorenas 1992). The swelling is in most cases caused by minerals of the smectite group, which most commonly originate from the weathering of feldspar. The hydration is adsorption of water due to the exchangeable cations between individual clay layers. Osmotic swelling happens between the grains and is driven by the ion concentration difference between grain surfaces and the pore water. The swelling takes place in two stages, with the hydration as the first, followed by the osmotic.

Both swelling and squeezing are common causes of tunnel convergence, and Einstein (1996) pointed out that these phenomena are often strongly interrelated and that one may lead to the other. He also provided short definitions for the two, where swelling is defined as the "*time-dependent volume increase of the ground, leading to inward movement of the tunnel perimeter*", and squeezing is defined as the "*time-dependent shearing of the ground, leading to inward movement of the tunnel perimeter*".

Creep is defined as deformations under constant load and occurs after or, under some conditions, at the same time as consolidation. It involves three phases: primary, secondary and tertiary. There are two types of creep associated with these phases: volumetric creep caused by volumetric stress and deviatoric creep caused by deviatoric stress. The primary creep phase is a result of volumetric creep and possibly deviatoric creep if the deviatoric stresses are large enough. Either the rate of strain during primary creep will fade out and the creep will stop, or it will decrease until the strain/time is constant. If the rate becomes constant, the creep process enters the secondary phase caused by deviatoric creep. Deviatoric creep is a time-dependent shear deformation caused by a serial change in the soil structure resulting from rearrangement of the grain contacts. If the creep rate increases rather than fading out, the process enters the tertiary phase. The tertiary phase is also caused by deviatoric creep and is important to avoid since it leads to failure.

In situ rock stresses are very important for determining which of the above processes will be dominant. Many researchers (Sheorey 1994; Hoek 2006; Herget 1988; Brown and Hoek 1978; Myrvang 2001) have found that the horizontal stresses near the surface are much larger than they would have been if they were only induced by gravitation. For a case where the ratio between horizontal and vertical stresses, k, is larger than 1, the stresses around the tunnel profile generally will be larger at the crown/invert than the walls. The initial parameters selected for the triaxial testing reported in this article are of a range corresponding to a tunnel with approximately $k = 2$ at a depth of approximately 50 m. An important point is that the tests do not try to fit these conditions or a stress path for an advancing tunnel exactly. The main intention is rather to investigate how the material reacts under the given conditions in order to observe whether swelling can be detected.

Some researchers, including Bellwald (1990), Aristorenas (1992) and Barla (1999), have done triaxial testing on weak rock materials, with focus on testing and tunnel deformation. Yeşil et al. (1993) and Bilir et al. (2008) have described triaxial apparatus and procedures with a focus on finding the swelling characteristics of clay-bearing rock. Wild et al. (2017) have described a multi-stage triaxial procedure for low-

permeability geomaterials. However, no literature describing research on the behaviour of swelling gouge material from weakness zones under triaxial loads has been found, and a procedure for investigating this issue, with the main focus on the swelling process, was therefore developed.

The testing was done on reconstituted cores of weakness zone material from four different locations in the eastern part of Norway. The material was dried before being reconstituted into cores using a compactor. The triaxial testing consisted of four main phases: 1) pre-stressing 1; 2) water addition under constant strain; 3) pre-stressing 2 and 4) failure.

In addition to testing of unconfined compressive strength (UCS), swelling pressure using an oedometer, and testing of free swelling, grain size distribution and density have been carried out.

The main objective of the triaxial testing described in this paper was to investigate whether swelling gouge material may exert pressure under typical in situ stress conditions or whether other processes may be dominant. An important objective was also to investigate the material properties, deformability and strength of the swelling gouge material. Very little information is currently available in the literature on these parameters, and increased knowledge will provide a better basis to estimate elastic and plastic deformation behaviour.

Test material characteristics

Bulk samples of weakness zone materials were collected at four different locations; see Table 1. The samples from Larvik and Drammen represent weakness zone gouge materials from Permian intrusive rocks, monzonite and granite, respectively. The Åsland and Bjørkelangen samples both represent weakness zone materials from Pre-Cambrian gneiss. See Fig. 2.

Swelling pressure and free swelling

Testing of swelling potential of the gouge material has been done according to Norwegian methodology developed at the Norwegian Universityof Science and Technology (NTNU), as described in Mao et al. (2011), Nilsen (2016) and others. Briefly explained, the fraction above 20 μm is removed by wet sieveing, and the remaining material is oven dried and milled into a fine powder. For the swelling pressure test, 20 g of material of the <20-μm fraction was placed in a 20-cm^2 steel ring and then compacted with a pressure of 2 MPa. The pressure was released, and after the expansion caused by the unloading had stopped, the height was set to be constant, and water was added. During the swelling process, no expansion of the material was permitted, and swelling pressure was determined as the final pressure build-up.

In the free swelling test, the material was prepared in the same manner as for the swelling pressure test described above. Ten millilitres of loosely packed material was poured into a 50-ml graded cylinder filled with distilled water, and the new volume was measured after sedimentation. The free swelling is the volume after sedimentation divided by the dry volume, given as a percentage.

The results of swelling pressure and free swelling tests are shown in Table 2. The swelling pressures obtained from oedometer tests are medium to high (0.1–0.3 MPa and 0.3–0.75 MPa, respectively), and the free swelling values are high and very high (140–200% and > 200%, respectively) according to Norwegian classification standards (NBG 1985). Differences in the categorization between the methods may come from different content of types of montmorillonite, especially Na-montmorillonite (Kocheise 1994).

Although the results in Table 2 are of value for classification and for evaluating swelling potential, it is important to note that these are only index tests, and due to sample preparation and discrepancies from in situ conditions, the resulting swelling pressures cannot be used directly for dimensioning of support structures.

Table 1 Localities of the different materials

Location number	Test location	Surrounding rock	County
1	Larvik	Monzonite	Vestfold
2	Åsland	Gneiss	Oslo
3	Bjørkelangen	Gneiss	Akershus
4	Drammen	Granite	Buskerud

Material grading

For the determination of material grading, wet sieving and sedimentation analysis (< 63 μm) was done according to Statens vegvesen (2016).

Material grains >4 mm were removed in order to facilitate homogeneity in the cores for triaxial testing. As indicated by the material grading curves in Fig. 3, this means that between 70 and 80% of the original material was included in the triaxial testing. As also shown by Fig. 3, materials 1, 2 and 4 have quite similar grain size distributions, while 3 has a larger portion of sand than the others. The material from location 1 is defined as gravely, sandy and clayey material, while locations 2, 3 and 4 are defined as gravely and sandy.

Density

Two different methods were used to determine the density, depending on the hardness of the sample. For soft materials, a density cylinder with a known volume was pushed into the material and weighed after oven drying according to Statens vegvesen (2016). See Fig. 4.

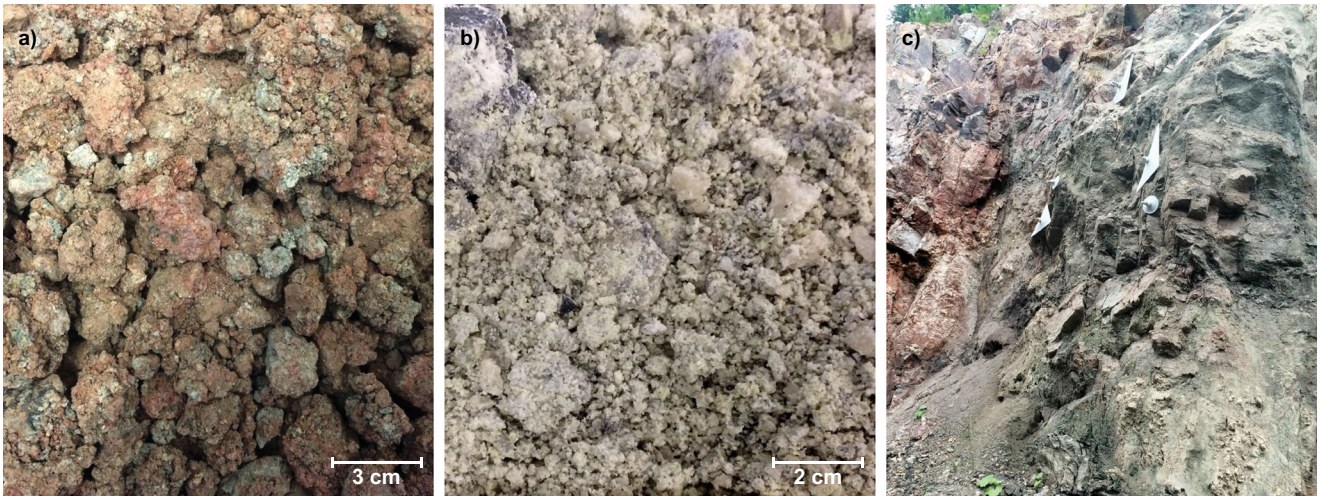

Fig. 2 **a**) Material from Larvik after collection; **b**) material from Åsland after collection; **c**) site of the Bjørkelangen material. The Drammen material is shown in Fig. 4

The more solid samples were submerged in water to find the volume. The water volume was determined from photos taken before and after submergence, in order to obtain the most accurate recording possible. The test pieces were weighed after drying and the density was calculated.

Density was measured on material from two of the locations, Drammen and Bjørkelangen (see Fig. 5). The Drammen material was tested both on soft material with a cylinder and on harder test pieces. For Bjørkelangen, only test pieces were used. In Table 3, the individual test values are presented. The averages of the different test series are 2.23 g/cm^3 for Bjørkelangen (sample piece), 2.14 g/cm^3 for Drammen (sample piece) and 2.00 g/cm^3 for Drammen (soft material).

Test methodology and equipment

Core preparation

To create solid cores of the gouge material, a compactor with an inner diameter of 54 mm was specially designed and produced for this study. The compactor was placed in a workshop hydraulic press with a 10-ton capacity, which provides a possible maximum pressure of 43 MPa. The compactor had pistons at the top and bottom, making it possible to apply pressure on both sides of the sample (see Fig. 6). A gauge was used to measure the axial deformation during loading.

Prior to the reconstitution of the gouge material into cores, particles larger than 4 mm were removed by wet sieving as described above. The material batches from each location were divided into suitable specimen sizes using a sample splitter. Before sample preparation, the material was dried at 60 °C for 24 h and taken out of the oven shortly before sample preparation. The finished cores were stored in a zip-lock plastic bag. During storage, the samples may have absorbed humidity from the air through the plastic. It is, however, believed to be very small amounts.

For the preparation of the cores, the following procedure was used:

1. Very cautious hand-grinding in a porcelain mortar to separate adhered material
2. Pouring the sample into the cylinder with the grain size kept as homogenous as possible throughout the process
3. Placing the cylinder in the press, lowering the press piston and removing the cylinder support at the bottom
4. Applying the load stepwise first to 0.5 ton, then to 1 ton and by increments of 1 ton up to 6 or 8 tons and waiting for deformations to stop between each step. Deformations were registered for each step.

Table 2 Swelling properties from oedometer and free swelling tests

Number	Location	Swelling pressure [MPa]	Swelling pressure classification	Free swelling [%]	Free swelling classification
1	Larvik	0.43	High	188	High
2	Åsland	0.18	Medium	142	High
3	Bjørkelangen	0.39	High	290	Very high
4	Drammen	0.21	Medium	180	High

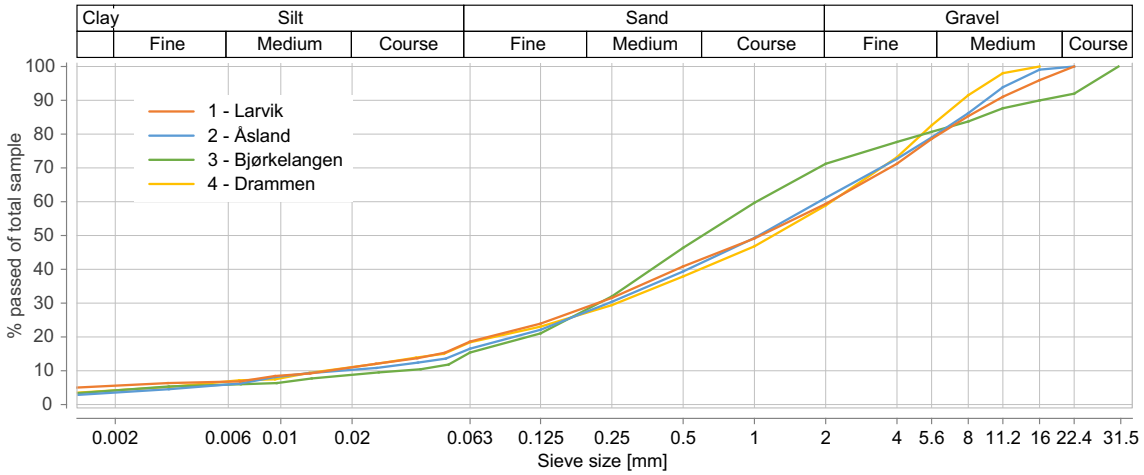

Fig. 3 Grain size distributions of the materials from the four different locations

5. Removing the bottom piston and extracting the core by applying load on the top. A load very close to the maximum preparation load was usually needed to push the core out of the cylinder.
6. Weighing the final core and measuring the length with a digital sliding calliper

Test rig

The rig used for uniaxial and triaxial testing was a GCTS RTR-4000 located at the Department of Geosciences and Petroleum, Norwegian University of Science and Technology. The machine is fully computer-controlled and has a maximum axial load capacity of 4000 kN and a maximum cell pressure of 140 MPa. The frame stiffness is 10 MN/mm. Axial deformation was measured with two linear variable differential transformer (LVDT) sensors placed at 180 degrees. Radial deformation was measured with one LVDT sensor mounted on a rolling chain placed at the centre (lengthwise) on the sample. The LVDT sensors had a range of 5 mm.

Uniaxial testing

The uniaxial testing was performed to obtain inputs on the mechanical properties of the reconstituted cores as a basis for determining the setup for triaxial testing. The test procedure was based on the method suggested by the International Society for Rock Mechanics (ISRM) for determining the uniaxial strength and deformability of rock materials (ISRM 2007).

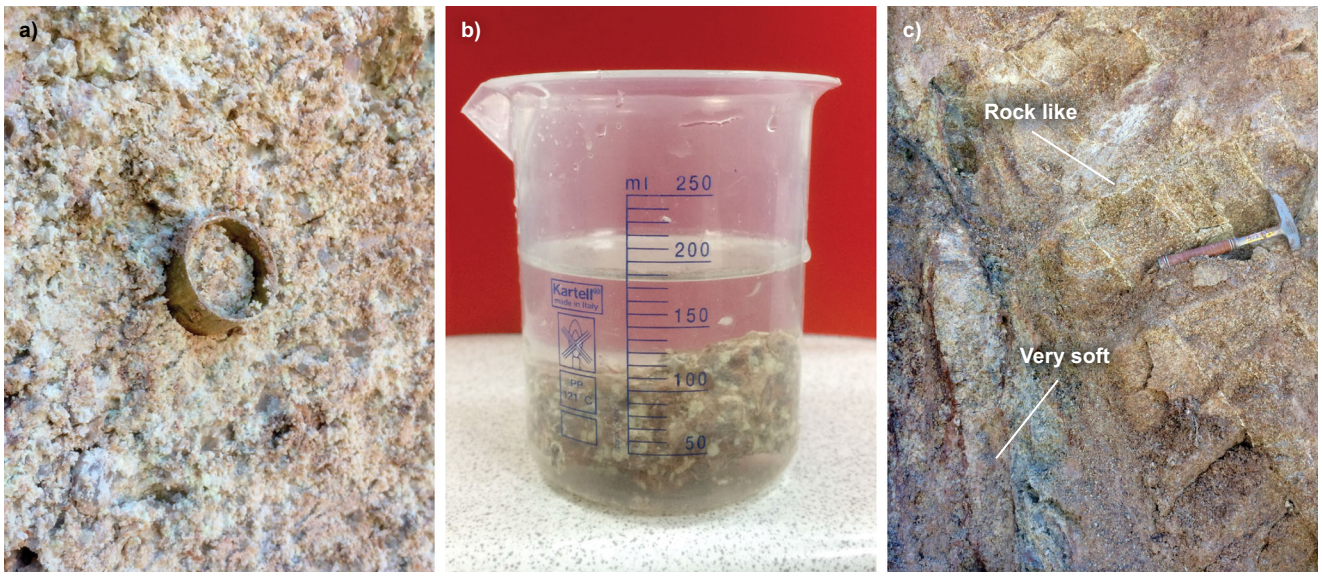

Fig. 4 Sampling density of different types of weakness zone materials. Samples in (**a**) and (**b**) were collected in the very soft and rock-like areas, respectively, both of which are marked in (**c**)

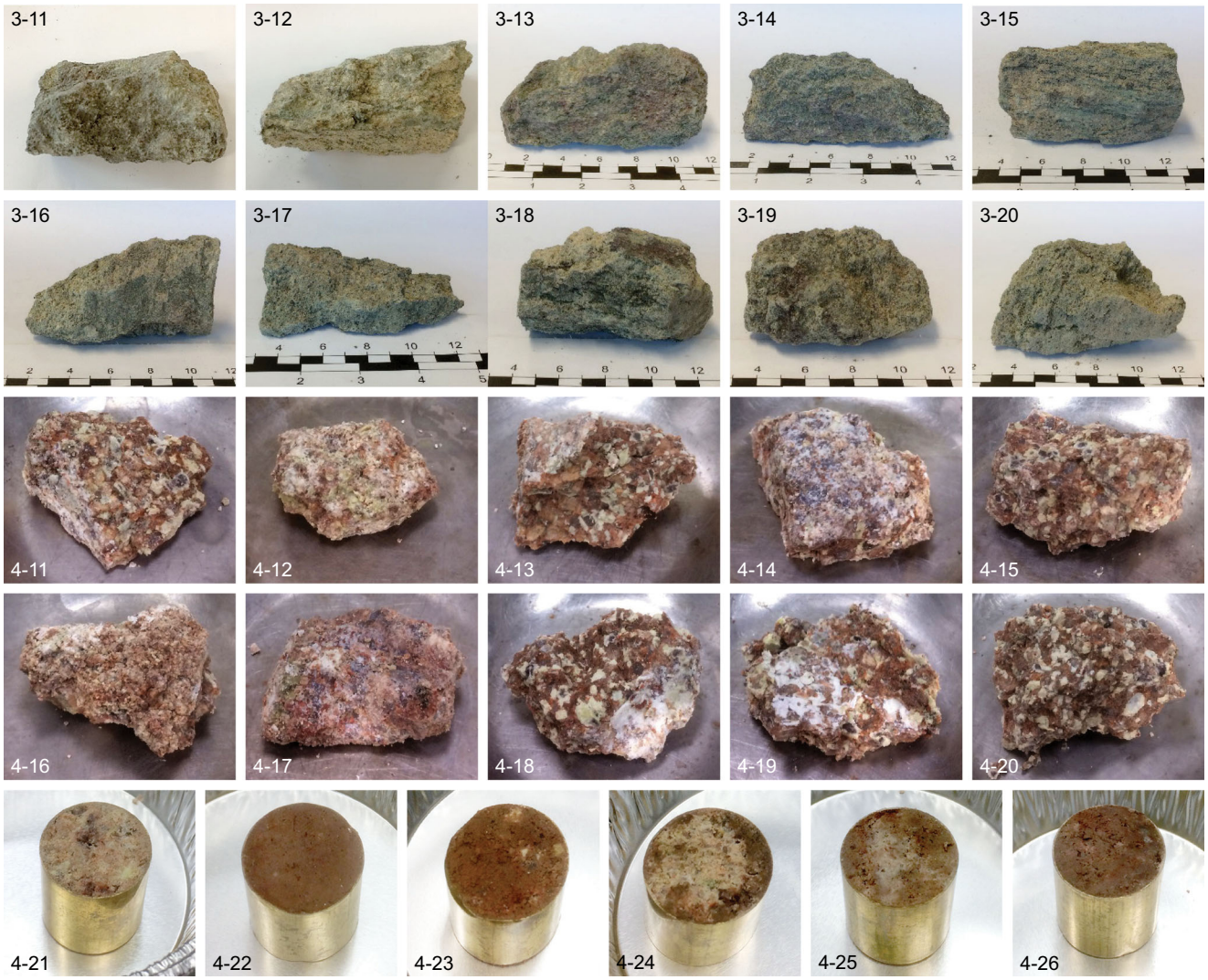

Fig. 5 Sample specimens used for the determination of density

To determine the E-modulus, the tangent modulus was utilized with ±15% of 50% of the UCS defining the regression line. Due to a jagged curve, a larger interval than the usual 10% was used.

To protect the equipment from dirt and dust, the test specimens were covered with a sleeve. For the first two UCS tests, a heat shrink sleeve was used, as in the procedure for the triaxial testing. For subsequent UCS tests, the heat shrink sleeve was switched with cling foil to see to what degree the results were affected by the confinement from the shrink sleeve and to ensure uniaxial behaviour.

Triaxial testing

Equipment

The test setup had some modifications regarding the distribution of water in the sample, where the standard setup is to let in water at the bottom end face of the sample and let it out at the top end face. Instead, the water was distributed to the sides of the samples by using specially designed end-pieces (see Fig. 7a) allowing it to flow along the sample in a non-woven casing (Fig. 7b). The water inlet was at the bottom of the sample, and the water outlet was at the top (Fig. 7c). The modified setup was designed to ensure a fast and outside-in soaking of the samples. The drainage valve was open through all stages to ensure as little pore pressure built up as possible. A test with an aluminium core was performed to estimate the additional radial deformation from the non-woven casing surrounding the sample.

The oil chamber surrounds the whole sample setup, making the cell pressure (S_c) act in both radial and axial directions. The deviator stress (σ_d) is the pressure acting from the axial piston. The radial stress (σ_r) is then the same as the cell pressure, and the axial stress (σ_a) is then equal to $S_c + \sigma_d$.

Table 3 Density of weakness zone material

Bjørkelangen, test piece				Drammen, test piece				Drammen, soft material			
Sample	cm^3	g	g/cm^3	Sample	cm^3	g	g/cm^3	Sample	cm^3	g	g/cm^3
3-11	80	170.4	2.13	4-11	35	79.8	2.28	4-21	6.2	12.4	2.02
3-12	74	167.4	2.26	4-12	15	35.6	2.38	4-22	6.1	12.4	2.04
3-13	100	232.3	2.32	4-13	40	85.3	2.13	4-23	6.1	12.3	2.02
3-14	60	134.8	2.25	4-14	40	73.7	1.84	4-24	6.2	12.0	1.96
3-15	88	207.2	2.35	4-15	36	83.6	2.32	4-25	6.2	12.1	1.96
3-16	104	236.2	2.27	4-16	39	67.3	1.73	4-26	6.1	12.2	2.00
3-17	52	116.2	2.23	4-17	21	40.3	1.92				
3-18	100	222.0	2.22	4-18	45	89.9	2.00				
3-19	93	198.8	2.14	4-19	22	52.4	2.38				
3-20	99	209.5	2.12	4-20	38	93.4	2.46				

Test procedure

The intention behind the selected test procedure was to investigate whether a build-up of swelling pressure might occur during water addition of a representative gouge material under a stress state that is relevant for typical tunnel projects. The test had four main phases, as described below and illustrated in Fig. 8.

(1) Pre-stress 1

Two different procedures for increasing the cell pressure and the deviator stress were used; simultaneous, pre-stress 1a (*P1a*), and sequential, pre-stress 1b (*P1b*):

- For *P1a*, both the cell pressure and the deviator stress were increased at the same time.
- For *P1b*, the cell pressure was first increased to its pre-set level, immediately followed by an increase of the deviator stress.

Before moving to the next phase, the pre-stress was held for some minutes to ensure stable behaviour.

(2) Water addition

The water addition phase started by switching from constant stress to constant strain. To observe the reaction of the switch, a pause of some minutes was taken before starting to add water. The goal was not to fully saturate the sample, but to make it sufficiently wet for the minerals to swell. The water was controlled manually to ensure a slow, constant flow along the sample. A minor pressure was needed to push the water through the non-woven fabric. To ensure that the effect of the water addition on the sample was as small as possible, i.e. to keep the effective stress the same as the total stress, the water pressure was kept below 0.15 MPa. The water addition was maintained until the sample was believed to be wet all the way through.

Since the strain was set to be constant, no expansion or contraction was allowed in either direction. If swelling occurred, the machine would then increase the axial and/or radial stress to keep the strain constant. Correspondingly, if the material tended to shrink, the machine would lower the axial and/or radial stress. The cell pressure was controlled by the radial strain, while the deviator stress was controlled by the axial strain. A close interaction between the two was therefore needed to ensure constant strain behaviour. The non-woven casing disturbs the constant strain for the actual core as the

Fig. 6 Setup for the compaction of the gouge material

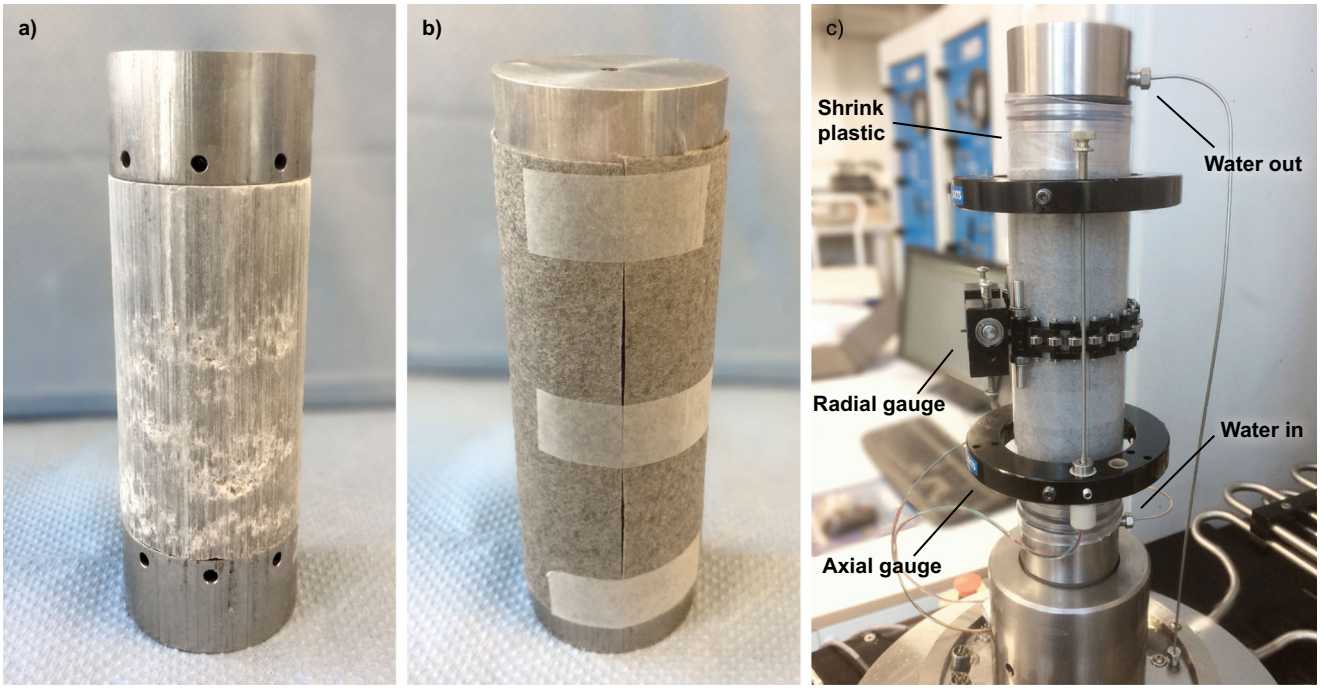

Fig. 7 Sample setup. **a**) New end-pieces to distribute water to the sides of the sample. **b**) A non-woven casing covers the sample and the holes in the water distributor. **c**) Ready for testing with the sample covered with a heat shrink sleeve and the water tubes and deformation gauges mounted

casing, to some degree, will expand with lowering of stresses and contract with increasing stresses, resulting in a reduced stress reduction or build-up. However, this effect is believed to be small as the allowed radial change of the core is estimated to be on a level below 0.1%.

(3) Pre-stress 2

As for the pre-stress 1 phase, simultaneous pre-stress 2a (*P2a*) and sequential pre-stress 2b (*P2b*) loadings were used. During water addition, a reduction of the cell pressure and the deviator stress occurred, and both were brought back up to 2 MPa.

(4) Failure

The cell pressure was reduced, making the sample fail, and the test ended when the axial strain reached 30,000 μS.

After testing, the sample was split to conduct a visual examination of whether it was fully soaked.

Parameter calculation

To calculate the E-modulus, the relationship between σ_d and ε_a was used. As for the uniaxial tests, a regression line for a part of the curve was used to find the E-modulus, as described in Section 0. For many of the tests there was nonlinear

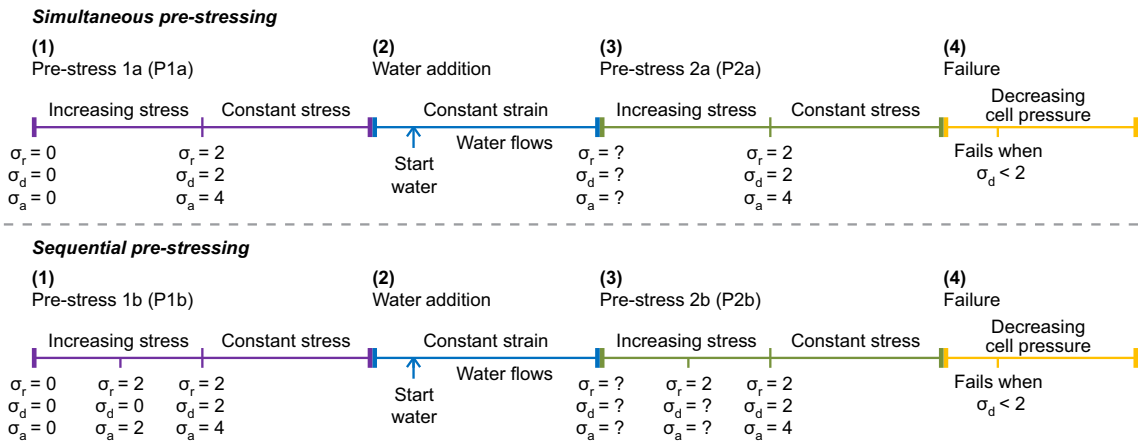

Fig. 8 Timeline for triaxial testing. The lengths of the lines are not representative of the time actually spent on a phase

behaviour, and in these instances the data at the end of the path were emphasized.

The strength parameters were found by using the software RocData (Rocscience Inc. 2015). As indicated in Fig. 8, the sample theoretically fails when the deviator stress is less than 2 MPa. For practical purposes, it seems that the deviator stress slowly started to decrease some time before failure. The point of failure was determined visually in the program combined with an evaluation of the residual error development. For these data, a residual error below 0.010, using the linear regression algorithm and vertical-relative error summation for the generalized Hoek-Brown criterion, seemed appropriate.

In phases 3 and 4, the unsaturated triaxial tests are performed with open drainage valves. As it is known that the pressure in the water phase is zero, and the air pressure is unknown, the strength and deformability parameters are determined from a total stress analysis. However, due to the deformation rate used, it cannot be guaranteed that no pore pressure was built up in these phases.

Results

Core preparations

The sample preparation was difficult and time-consuming. The most significant problem was that the core got stuck in the cylinder if the maximum load was too large. Therefore, both 6 and 8 tons (representing 26 and 34 MPa, respectively) were used as maximum loads to make the samples. The respective physical properties of the test samples are shown in Table 4. It is believed that the cores have a relatively uniform degree of compaction throughout the sample, but due to friction between the sample and the preparation cylinder, the density is believed to be slightly lower in the middle than on the ends.

Uniaxial testing

Only sample series 3 and 4 were subjected to uniaxial testing in order to save samples from series 1 and 2 for triaxial testing. Samples 3-2 and 3-3 were tested covered with a heat shrink sleeve, while the rest were loosely wrapped with cling foil. As seen in Fig. 9, samples 3-2 and 3-3 have a considerably greater strength that most likely comes from the radial confinement caused by the heat shrink sleeve. The values for UCS and E-modulus are shown in Table 5.

Triaxial testing

Eight triaxial tests were performed: four with *P1a* and *P2a*, one with *P1a* and *P2b* and three with *P1b* and *P2b*. Plots for all tests are not shown in this article since they would require too much space. For additional plots and the raw data, reference can however be made to Online Resource 1.

Testing with aluminium cores showed that the non-woven casing adds a strain of approximately 2500–3000 μS when the cell pressure is 2 MPa, with a creep of approximately 70 μS for 30 min. When the pressure was lowered, the casing showed a (negative) strain of approximately 1300 μS for

Table 4 Physical properties of the samples

Sample number	Diameter [mm]	Length [mm]	Mass [g]	Density [g/cm^3]	Max. load [10^3 kg]	Comment/use[a]
1-5	54	114.79	532.9	2.03	6	Triaxial/pre-stress b
1-6	54	115.75	542.9	2.05	6	Triaxial/pre-stress a
2-8	54	112.02	520.6	2.03	8	Triaxial/pre-stress a
3-2	54	108.01	477.5	1.93	6	Uniaxial (hss)/compacted one side only
3-3	54	106.57	487.9	2.00	8	Uniaxial (hss)
3-4	54	110.74	506.2	2.00	8	Uniaxial (cf)
3-6	54	106.49	490.4	2.01	8	Triaxial/pre-stress a
3-8	54	107.17	495.9	2.02	8	Triaxial/pre-stress b
4-1	54	112.27	514.0	2.00	6	Uniaxial (cf)
4-2	54	107.08	490.6	2.00	6	Uniaxial (cf)
4-3	54	112.40	518.3	2.01	8	Uniaxial (cf)
4-4	54	100.94	468.4	2.03	8	Uniaxial (cf)
4-5	54	101.76	482.3	2.07	8	Triaxial/pre-stress a
4-8	54	102.07	480.2	2.05	8	Triaxial/pre-stress b
4-9	54	101.92	483.2	2.07	8	Triaxial/pre-stress 1b and 2a

[a] Uniaxial testing with heat shrink sleeve is marked "hss" and cling foil is marked "cf"

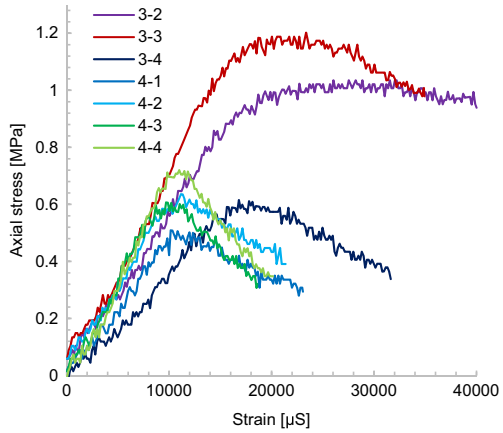

Fig. 9 Uniaxial testing. Samples 3-2 and 3-3 were covered with a heat shrink sleeve, while the rest were wrapped in cling foil

2 MPa. There was no change in strain observed due to the wetting of the non-woven fabric.

Observations from specimens that were not completely saturated indicate that the waterfront moved, as shown in Fig. 10. As most of the unsuccessful tests were on samples treated with pre-stress procedure *a*, this may differ for samples treated with pre-stress procedure *b*. Figure 11 shows a sample after testing that was split with a knife to check whether the water addition was successful.

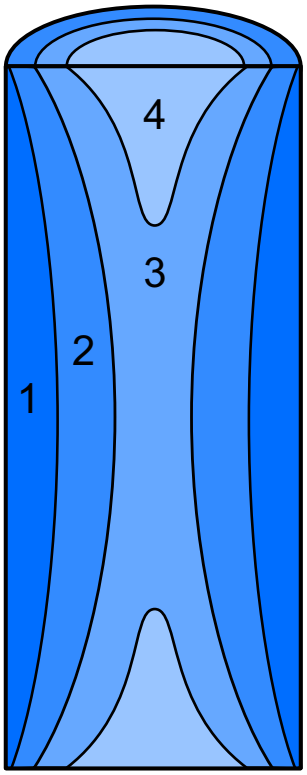

Fig. 10 Probable movement of the waterfront of the samples during water addition (with increasing numbers)

Pre-stressing and creep

The test results for the two different pre-stress procedures showed quite different behaviour. The behaviour was however quite similar within each of the different procedures. Two test series representing each procedure are therefore presented: sample 2-8 (pre-stress *a*) and 4-8 (pre-stress *b*). In Figs. 12 and 13, the test series are presented as stress and strains against time. In Figs. 14 and 15, the development of τ_{max}, which is the top of the Mohr circle, is plotted for each phase.

After the stresses peaked, one could observe a slow increase in the strains. This is believed to be creep, as described in Section 0, due to the rearrangement of the grains in the skeleton under constant stresses. In phase 2, the strains are set to be constant. The consequence of the creep in a state of constant strain will be a reduction of the stresses, as the sample will not push back as much as before when the grains rearrange themselves.

For pre-stress procedure *a*, one can observe a small creep in the axial and radial direction. After the switch to constant strain, one can see that the cell pressure decreases while the deviator stress stays at the same level. This indicates that the creep is volumetric.

For pre-stress procedure *b*, one can see that the creep in the axial direction is much larger than in the radial direction. In

Table 5 Material properties from uniaxial testing

Sample number	Preparation load [10^3 kg]	UCS [MPa]	E-module [MPa]
3-2	6	1.04[a]	62.6[a]
3-3	8	1.20[a]	78.3[a]
3-4	8	0.62	43.7
4-1	6	0.51	48.5
4-2	6	0.64	57.4
4-3	8	0.61	85.5
4-4	8	0.72	77

[a] Samples with heat shrink sleeve

Fig. 11 Test sample 2-8 split after testing to check quality of water addition. In the case of dry zones, they were easy to detect

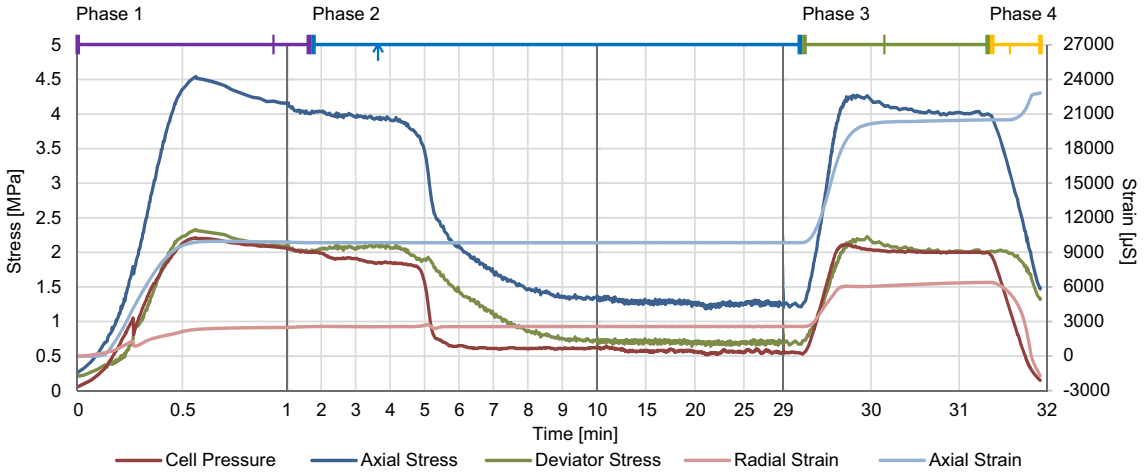

Fig. 12 Stress and strains against time for sample 2-8. Phases, including sub-events, are seen at the top of the chart and correspond to Fig. 8. The flow of water is started at the blue arrow

Fig. 13, one can see at about the 30-min mark that the decrease in cell pressure is evening out and the deviatoric stress is still decreasing. This indicates that the creep has entered its secondary phase with deviatoric creep.

In Table 6, the strains at the end of phase 1 are listed with the initial and new density of the different samples. One can see that the strains are considerably larger for the samples pre-stressed with the *b* procedure than those pre-stressed with the *a* procedure, which also resulted in a larger density for these samples.

Water addition and possible swelling

In Figs. 12 and 13, the small arrow on the blue line at the top indicates the point of time at which the water started to flow. An increase in the stresses after adding the water was not observed in any of the eight samples, but rather a decrease of both axial and radial stresses. This does not necessarily mean that no swelling occurred, but rather that due to the water saturation, or as a result of the swelling, other processes were dominant.

In Fig. 14 (phase 2) for sample 2-8, and also in general for the samples that underwent pre-stress procedure *a*, one can see that the path is horizontal and moving to the left before it starts to decline. In the horizontal part, it is believed that the normal stress, σ_n, needed to sustain the radial and axial strain is decreasing. Where the line starts to decline, the shear stress, τ_θ, limit is also met, which indicates that the failure envelope is changing (getting lower), as indicated in the figure. In other words, the friction angle, φ, and cohesion, c, seem to become lower.

In the saturation phase, the samples that underwent pre-stress *b* showed quite different behaviour (Figs. 13 and 15 (phase 2)). The creep in the axial direction in the constant stress part of phase 1 was quite large, while the radial strain was smaller, but still larger than for pre-stress *a*. When

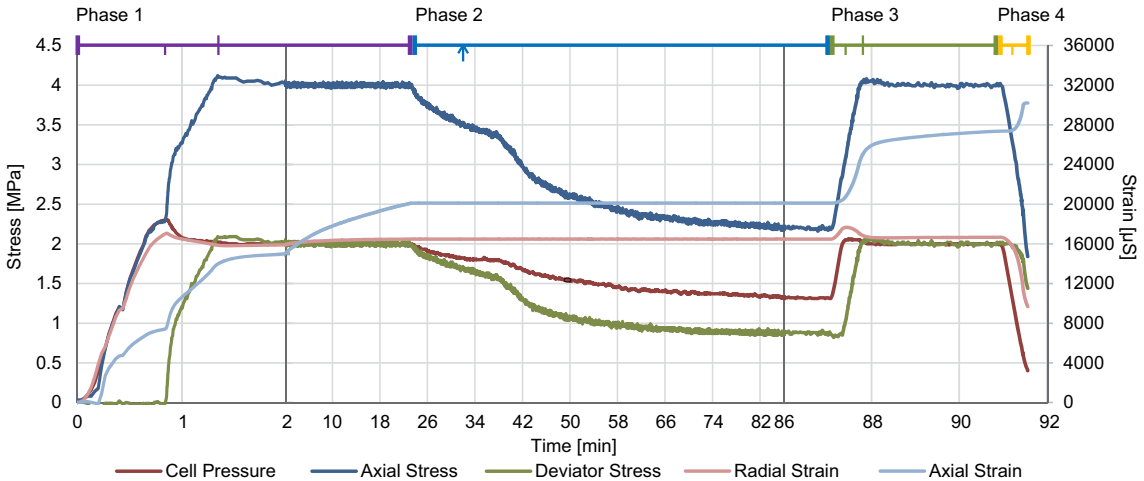

Fig. 13 Stress and strains against time for sample 4-8. Phases, including sub-events, are seen at the top of the chart and correspond to Fig. 8. The flow of water is started at the blue arrow

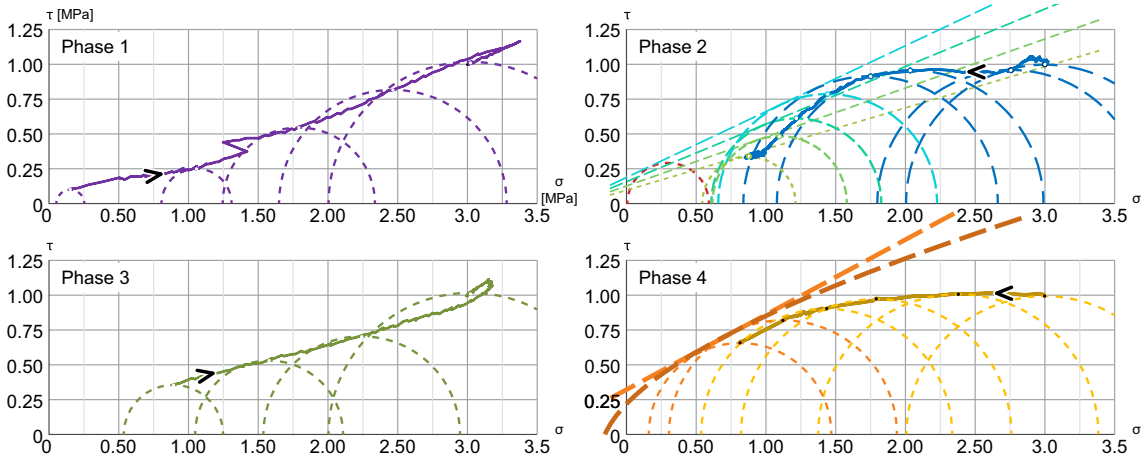

Fig. 14 Stress states illustrated with Mohr circles for sample 2-8 in the different phases. The arrows indicate the direction of progress. The failure envelopes shown for phase 2 are only suggested/illustrative, while for phase 4, they are calculated in RocData (Rocscience Inc. 2015). The straight line is Mohr-Coulomb and the curve is Hoek-Brown. The red half-circle in phase 2 represents an average value from UCS tests

switching to constant strain in phase 2, this creep resulted in a quite significant reduction of the axial stress and a smaller reduction in the radial direction. The water required more time to saturate the sample, and the reaction was slower than for the pre-stress *a*. For one sample, 3-8, it was difficult to see any reaction at all from the saturation. In sample 4-8, one can see from Fig. 15 that the rate of stress reduction increases when the water starts saturating the sample. Accordingly, no swelling pressure is observed. The reduced stresses of all samples at the end of phase 2 are listed in Table 7.

E-modulus

The stress/strain curves used to find the E-modulus are presented in Fig. 16, and the resulting values are listed in Table 8. Compared to the uniaxial tests, one can see that the values from the triaxial test are a bit higher. It does not seem to be a significant difference between the pre-stressing procedures, but it does seem that the values are generally lower on the second pre-stressing.

Strength

The strength properties of the samples are listed in Table 9. The stress range for finding these values is quite small, at least for tunnel applications, and the line fitting is therefore quite sensitive to small variations in the raw data. One should therefore be extremely cautious about using such values outside the tested stress range, and one should also bear in mind that the samples are reconstituted cores.

The Hoek-Brown m_i value is a material constant and depends upon the frictional characteristics of the component minerals (Hoek and Marinos 2000). The m_i values for 3-6 in particular, but also 3-8 and 4-8, seem too high compared to

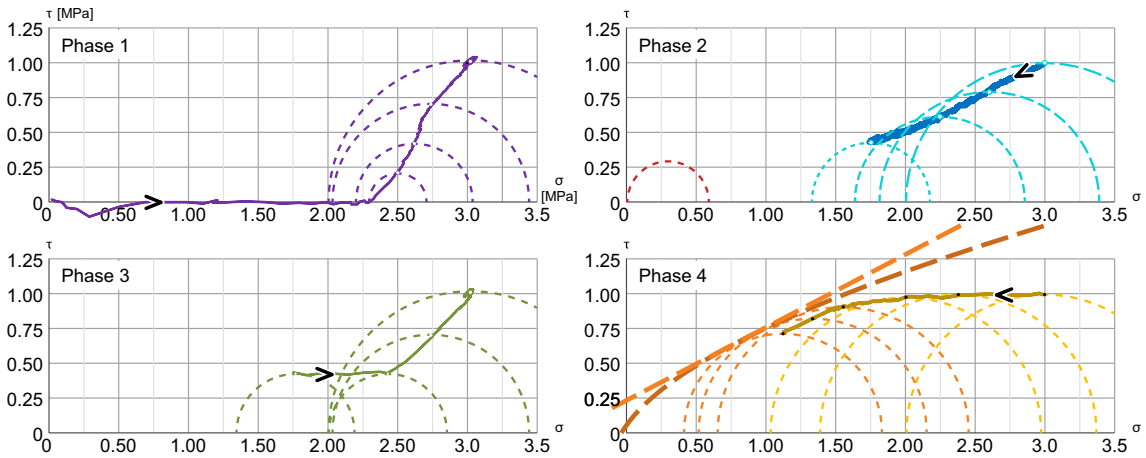

Fig. 15 Stress states illustrated with Mohr circles for sample 4-8 for the different phases. The arrows indicate the direction of progress. The failure envelopes in phase 4 are calculated in RocData. The straight line is Mohr-Coulomb and the curved is Hoek-Brown. The red half-circle in phase 2 represents an average value from UCS tests

Table 6 Strains and density of the samples at the end of phase 1

Sample number	Pre-stress procedure	Axial strain, ε_a [μS]	Radial strain[a], ε_r [μS]	Volumetric strain, ε_v [μS]	Initial density [ton/m^3]	New density [ton/m^3]
1-6	a	7688	6943	21,420	2.05	2.09
2-8	a	9881	2504	14,834	2.03	2.06
3-6	a	11,117	7972	26,822	2.01	2.07
4-5	a	7719	4325	16,283	2.07	2.10
1-5	b	9764	18,708	46,469	2.03	2.13
3-8	b	21,318	18,799	57,769	2.02	2.14
4-8	b	20,109	16,476	52,133	2.05	2.17
4-9	b	14,739	17,301	48,536	2.07	2.18

[a] Not corrected for strain from the non-woven casing

empirical values, where weak and soft rocks have values of approximately 7 and lower (Hoek and Marinos 2000). Looking at the friction angle, samples 3-6 and 3-8 also stand out with high values, but sample 4-8 has one of the lowest values. For more information on this, reference is made to Online Resource 1.

Discussion

The experiment setup was designed mainly to investigate whether a swelling gouge material is likely to exert pressure when exposed to water in a probable and typical stress situation. Since it is very difficult to obtain samples of undisturbed material, reconstituted cores were used.

The main challenge of using reconstituted cores is to recreate the properties of in situ material. The macrofabric of the sample material was possible to study visually, and when splitting the samples after testing (see Fig. 11), the observations indicated that the samples had a quite even distribution of grain sizes. Such even distribution is not the case for most in situ gouge materials, for which accumulation of, e.g., fine grains are often found between the larger fragments (see Fig. 4a).

Table 7 Stresses at the end of phase 2

Sample number	Pre-stress procedure	σ_a [MPa]	σ_r [MPa]	σ_d [MPa]
1-6	a	0.8	0.3	0.6
2-8	a	1.2	0.6	0.7
3-6	a	1.6	0.9	0.7
4-5	a	0.9	0.5	0.5
1-5	b	1.7	0.9	0.8
3-8	b	2.8	1.6	1.2
4-8	b	2.2	1.3	0.9
4-9	b	1.5	0.9	0.6

The porosity, or occurrence of voids, in the material may be expressed as a function of the density. After the first pre-stressing (phase 1), the samples had a density of 2.06–2.18 g/cm^3, with the highest values for the samples pre-stressed with procedure *b* (see Table 6). For two of the locations, the density of in situ material was tested, resulting in average values of 2.23 g/cm^3 (test piece) for the Bjørkelangen location and 2.00 g/cm^3 (soft material) and 2.14 g/cm^3 (test piece) for Drammen (see Table 3). These densities are at levels similar to those for the sample cores after preparation (see Table 4) and after phase 2. Based on this similarity, it is assumed that the density, which is correlated with the pore volume, of the samples is quite similar to the in situ material. As stated in the introduction, the bonding between the grains for this type of material in situ is believed to be low to non-existent. Both the in situ material and the compacted cores are on the verge of disintegrating when handled and are apprehended as being similar.

A main difference from in situ conditions is that the laboratory-tested samples were dry, while in situ material has an initial water content. This implies two potential main objections: 1) the material properties may be different when the material is wet, and 2) the material has already, to an uncertain degree, swelled when wet. These objections are relevant not only for reconstituted cores, but also for "natural" in situ samples used in a laboratory.

None of the triaxial tests showed increased pressure during water addition indicating the build-up of a swelling pressure. The materials had medium and high swelling pressure obtained by oedometer testing of material <20 μm.

When performing the tests, one could immediately observe a creep behaviour after the stabilization of the stress in phase 1. Creep is originally defined as deformations at a constant load, caused by a serial change in the structure through a rearrangement of the soil contacts (Havel 2004). However, this creep could be observed as a slow decrease of the applied stresses under constant strain in phase 2 before the water addition.

For pre-stress procedure *a*, a sudden reaction with a drop in the applied stresses occurred when the sample was saturated. This implies that the material does not need the same stresses to be held in place. As outlined in Fig. 14 (phase 2), this may be due to a lowering of the friction angle that comes from changes in the contacts between the grains caused by water or swelling. It seems that the material first creeps and then enters a state of shear failure at the same time as the friction angle drops. Since the saturation takes place radially, as outlined in Fig. 10, the sample is not homogenous during saturation as it has a decreasing core of dry material that can "withstand" the axial pressure.

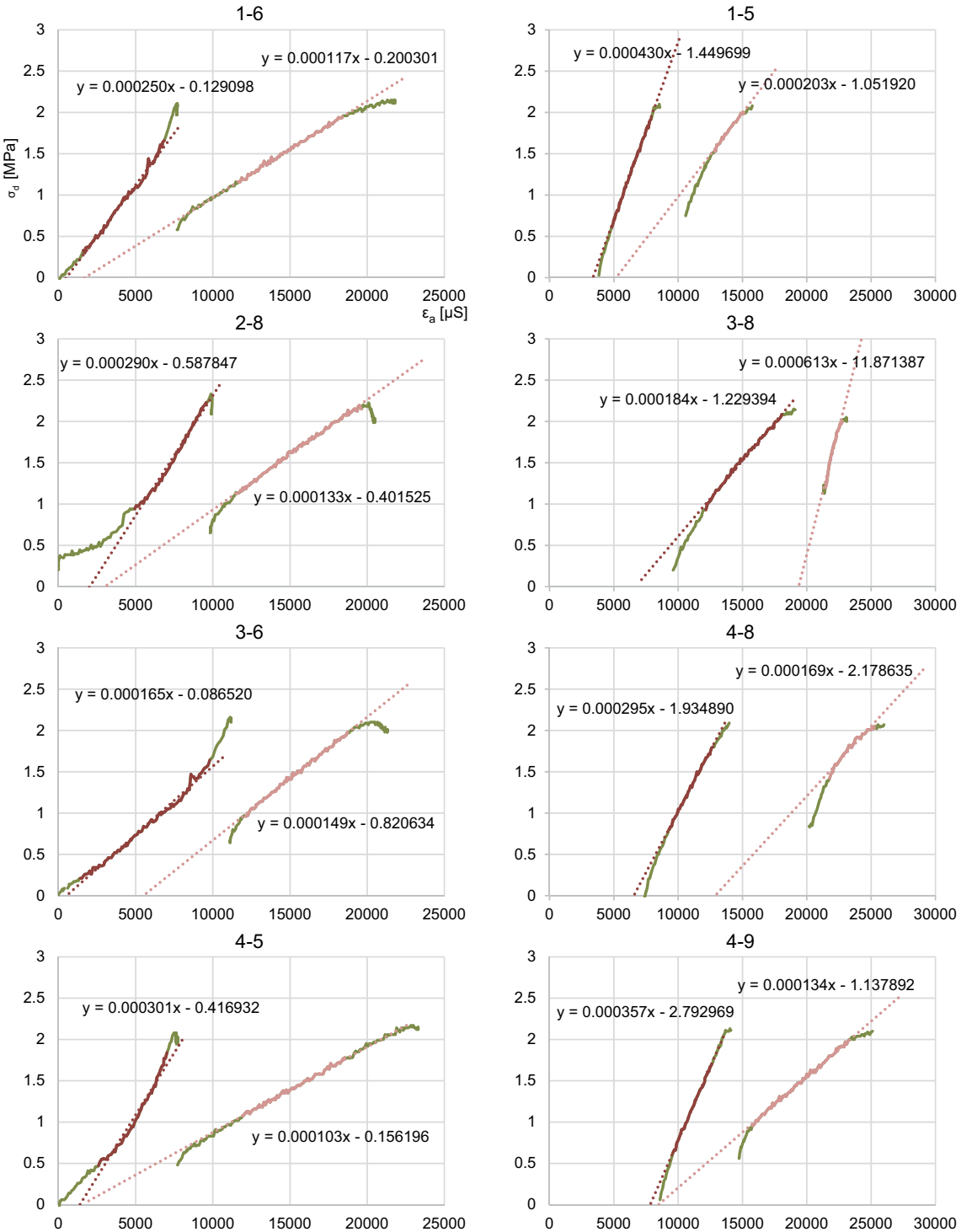

Fig. 16 Curves for the calculation of the E-modulus. The left curve (dark red) is from phase 1, and the right curve (light red) is from phase 3

Also, for pre-stress procedure *b*, the stresses decrease in phase 2, but generally at a slower pace, and the effect of the water is not that obvious, and for some samples, almost invisible. For the pre-stress *b* samples, it almost seems as though the water is a "catalyst" of the creep, as in Fig. 15 (phase 2). As shown in Table 6, the strain after phase 1 is generally higher for the pre-stress *b* samples. This indicates that the samples are more compact, which also probably makes the water move slower in the sample.

Because of the different properties of the pre-stress *b* samples, it seems that they do not enter a state of shear failure during water addition as the pre-stress *a* samples did.

Table 8 E-modulus from the triaxial test in phase 1 and phase 3

Sample number	Pre-stress procedure	E-modulus phase 1 [Mpa]	E-modulus phase 3 [Mpa]
1-6	a	250	117
2-8	a	290	133
3-6	a	165	149
4-5	a	301	103
1-5	b	430	203
3-8	b	184	613[a]
4-8	b	295	169
4-9	b/a	357	134

[a] Not a probable value. See discussion

The non-woven casing allows the sample to have an unintentional possibility to deform radially during phase 2. As the casing may expand when the stresses is lowered, the core may have a small radial contraction, causing a higher end pressure than if the casing was not there. It is not believed that this effect is very large, at least for most of the samples. This is because the maximum strain from this effect is probably about 1300 μS for a reduction of 2 MPa, and the strains during pre-stressing show that the deformability of the samples in such a stress range is far higher. Even with this being a significant effect, it is believed that it does not affect the behaviour in a way that influences the general interpretations of the results, as it only reduces the stress reduction.

The differences between volumetric and deviatoric creep may explain the different results in creep after the pre-stress procedures *a* and *b*. For procedure *a*, where the cell (volumetric) stress was applied at the same time as the deviatoric stress, a quite even creep in the radial and axial direction was observed. For procedure *b*, where the deviatoric stress was applied after the cell (volumetric) stress, an obviously larger axial (deviatoric) creep was observed.

Table 9 Strength parameters calculated by RocData (Rocscience Inc. 2015)

Sample	Pre-stress procedure	Generalized Hoek-Brown		Mohr-Coulomb	
		σ_{ci} [MPa]	m_i	Cohesion [MPa]	Friction angle
1-6	a	1.1	6.1	0.34	29.7
2-8	a	1.0	5.9	0.32	28.2
3-6	a	0.3	32.4	0.19	36.0
4-5	a	0.9	6.9	0.30	30.6
1-5	b	1.1	5.7	0.34	29.0
3-8	b	0.6	11.9	0.23	34.4
4-8	b	0.4	14.0	0.23	27.5
4-9	b/a	0.8	7.5	0.29	29.0

The situation where the strain is constant in phase 2 is not transferable to the situation in a tunnel, where the rock stresses will continue to push as the material creeps. If the same test was performed with constant stresses in phase 2, one would obtain better data to determine whether the creep—or the shear failure process—would be dominant in the different cases. As shear failure can result in the squeezing of the rock mass, the difference between creep and shear failure may have a significant influence on the tunnel excavation.

For the E-modulus (see Fig. 16 and Table 8), the values are generally lower after the water addition than before, except for the samples from location 3. Looking at the material grading curves (Fig. 3), one can see that the location 3 material has lower clay and silt content and higher sand content than the rest of the locations. This may make it less sensitive to the water addition. The E-modulus values obtained in the triaxial tests were higher than the E-modulus values obtained from the uniaxial tests, which is believed to be due to the increase in compaction from the pre-stressing itself and/or the radial support.

The creep will displace the curves for the second pre-stressing to the right, as sample 4-8 illustrates (see Fig. 16, 4-8 and Fig. 13, axial strain in phase 1). If one subtracts the creep for sample 3-8, the strain level would be almost the same after the second pre-stress. This indicates that the decrease of stress in the constant strain phase mainly comes from creep and not a change in the E-modulus. The E-modulus will then be invalid as the stress-strain curve defining it only gets back to the starting point. This also seems to apply to some degree for sample 3-6.

The change in the E-modulus implies an alteration of the material on a grain size level. Since it seemed that the pre-stress *a* samples experienced a shear failure in phase 2, it is believed that this contributed to the change. The stresses of the pre-stress *b* samples seemed to move below the failure envelope, but still experienced an E-modulus change. The expansion of the swelling clay minerals may have sped up and enhanced the creep deformation by affecting the grain contacts. Because there are voids in the samples, the swelling does not necessarily make the material expand, as grains move because of the swelling; they may rather collapse under the applied stress, making the sample smaller. However, samples without swelling material have not been tested, and the effect of swelling versus wet grains and grain contacts is difficult to define.

For the test results presented in Table 9, one should in particular be aware of the strength parameters for 3-6, 3-8 and 4-8, where the m_i value is higher than expected for these kinds of samples. In addition, these samples have the lowest σ_{ci} of all the samples, which also indicates that the failure envelope is too steep.

Conclusions

Based on the triaxial tests presented in this paper, it seems that there are factors other than the swelling pressure which may be the main reason for tunnel deformation to occur during excavation through a weakness zone containing swelling gouge. The low strength and low E-modulus of the gouge are believed in many cases to be major sources of deformations (elastic and plastic). For the time-dependent deformations, water is a key factor. If the material is fully saturated, water will be exerted, and the material will consolidate before possible creep occurs. Creep properties seem to be very important, and this phenomenon may cause failure by itself or combined with other processes. The deformation at one location causes a redistribution of the stresses around the tunnel over time that may initiate new deformation processes at places that were previously stable.

A main purpose of the triaxial testing described in this paper was to investigate strength and deformation parameters for swelling gouge materials, for which no previous data were found available in the literature. Valuable additional knowledge has been obtained based on the testing described here, but it should be emphasized that the E-modulus values and strength parameters achieved using the method presented in this paper should be applied with great care for engineering purposes as they are based on a limited stress range and performed on reconstituted samples.

References

Aristorenas GV (1992) Time-dependent behavior of tunnels excavated in shale. Dissertation, Massachusetts Institute of Technology, Cambridge

Barla M (1999) Tunnels in swelling ground: simulation of 3D stress paths by triaxial laboratory testing. Dissertation, Politecnico di Torino, Torino

Bellwald P (1990) A contribution to the design of tunnels in argillaceous rock. Dissertation, Massachusetts Institute of Technology, Cambridge

Bilir ME, Sari D, Muftuoglu Y (2008) A computer-controlled triaxial test apparatus for measuring swelling characteristics of reconstituted clay-bearing rock. Geotech Test J 31(4):535–541. https://doi.org/10.1007/978-3-319-09060-3_85

Brown ET, Hoek E (1978) Trends in relationships between measured in-situ stresses and depth. Int J Rock Mech Min 15(4):211–215. https://doi.org/10.1016/0148-9062(78)91227-5

Einstein HH (1996) Tunnelling in difficult ground - swelling behaviour and identification of swelling rocks. Rock Mech Rock Eng 29(3):113–124. https://doi.org/10.1007/bf01032649

Havel F (2004) Creep in soft soils. Dissertation, Norwegian University of Science and Technology, Trondheim

Herget G (1988) Stresses in rock. Balkema, Rotterdam

Hoek E (2006) Practical rock engineering. www.rocscience.com

Hoek E, Marinos P (2000) Predicting tunnel squeezing problems in weak heterogeneous rock masses. Tunnels & Tunnelling International vol November and December 2000. Polygon Media Ltd, London

ISRM (2007) The Complete ISRM Suggested Methods for Rock Characterization, Testing and Monitoring: 1974–2006. ISRM Turkish National Group, Ankara

Kocheise R-C (1994) Swelling clay in sub-sea tunnels. Dissertation, Norwegian Institute of Technology, Trondheim

Mao D, Nilsen B, Dahl F (2011) Laboratory Testing of Swelling Gouge From Weakness Zone - Principle And Recent Update. Paper presented at the 45th U.S. Rock Mechanics / Geomechanics Symposium, San Francisco, 26–29 June

Myrvang AM (2001) Bergmekanikk. Norwegian University of Science and Technology, Department of Geology and Mineral Resources Engineering, Trondheim

NBG (1985) Ingeniørgeologi Berg. Tapir, Trondheim

Nilsen B (2016) Reliability of swelling pressure testing for tunnel support evaluation. Paper presented at the ITA-AITES World Tunnel Congress 2016, San Francisco, April 22–28

Rocscience Inc. (2015) RocData. vol 5.003, 5.006 edn. Rocscience Inc., Toronto

Rokoengen K (1973) Swelling properties of clayey zones in rock. Dissertation, Norwegian Institute of Technology, Trondheim

Selmer-Olsen R (1985) Method for determination of dimensional swelling pressure. Paper presented at the Fjellsprengningskonferansen, Oslo, November 21–22

Sheorey PR (1994) A theory for in situ stresses in isotropic and transverseley isotropic rock. Int J Rock Mech Min 31(1):23–34. https://doi.org/10.1016/0148-9062(94)92312-4

Statens vegvesen (2016) Laboratory methods. vol R210. Statens vegvesen, Vegdirektoratet, Oslo

Terzaghi K, Peck RB (1967) Soil mechanics in engineering practice, 2nd edn. Wiley, New York

Wild KM, Barla M, Turinetti G, Amann F (2017) A multi-stage triaxial testing procedure for low permeable geomaterials applied to Opalinus clay. J Rock Mech Geotech Eng 9(3):519–530. https://doi.org/10.1016/j.jrmge.2017.04.003

Yeşil MM, Paşamehmetoğlu AG, Bozdağ T (1993) A triaxial swelling test apparatus. Int J Rock Mech Min 30(4):443–450. https://doi.org/10.1016/0148-9062(93)91725-X